

Optimization of The Electrospinning Process for Preparation of Nanofibers From Poly (Vinyl Alcohol) (PVA) and *Chromolaena odorata* L. Extract (COE)

I. Sriyanti^{1,2*}, L. Marlina¹, J. Jauhari²

¹Physics Education, Faculty of Education, Universitas Sriwijaya, Indonesia

²Laboratory of Instrumentation and Nanotechnology Applications, Faculty of Computer Science, Universitas Sriwijaya, Indonesia

Received: 24 January 2020. Accepted: 18 March 2020. Published: 30 June 2020

ABSTRACT

The *Cromaloena odorata* (COE) contains phenols, flavonoids, tannins, alkaloids, saponins, steroids that possess diverse therapeutic effects. However, COE has poor solubility in water and poor absorption in the body. Incorporation of COE in nanofiber system is a promising way to increase CEO solubility. One of the methods to produce nanofiber is electrospinning. The electrospinning process there are three of the most important process parameters are applied flowrate, voltage and TCD. In this study we developed optimized condition for electrospinning process of polyvinyl alcohol (PVA)/CEO and their characterization. The Scanning electron microscopy (SEM) analysis showed that modification of flowrate and TCD did not affect the morphology of PVA and COE fiber. However fiber diameter decreased when lower flowrate, higher voltage was applied, and TCD. Fourier Transform Infrared (FTIR) study was conducted to identify possible intermolecular interaction between PVA/COE that has potential application as antimicrobial wound dressing.

Keywords: Applied Flowrate; *Chromolaena odorata* Extract; Polyvinyl Alcohol; Tip-Collector Distance; Voltage

INTRODUCTION

Vinyl polymers such as Polyvinylidone (PVP), polyvinylacetate (PVAc), and polyvinylalcohol (PVA) have been widely used for transdermal dressings and drug delivery devices (Park, Lee, & Bea, 2008; Rasekh et al., 2014; Charernsriwilaiwat, Rojanarata, Ngawhirunpat, Sukma, & Opanasopit, 2008). The former polymer is of particular interest since it is a hydrophilic polymer with excellent biocompatibility, spinnability, aqueous solubility and easiness for electrospinning process. Polyvinyl alcohol has demonstrated effectiveness on controlling drug release and improving drug bioavailability of synthetic or natural compounds like emedion (Dai et al., 2012) and curcumin (Rahma et al., 2016).

Cromaloena Odorata L is a popular leaf among Southeast Asians, including Indonesia. There has been a growing interest in *croma-*

loena odorata leaf as herbal remedies for inflammation and infection. *Cromaloena odorata* leaf has been reported to contain phenols, flavonoids, saponins, terpenoids, tannins and steroids (Benjamin, 2015; Putri, & Fatmawati, S. 2019; De Oliveira, Bernardi, & Balbinot, 2017). Pharmacological activities of *Cromaloena odorata* leaf is in a wide range, from antifungal (Naidoo, Coopoosamy, & Naidoo, 2011), antioxidant (Handayani, Umar, & Ismail, 2018), Anti-plasmodial (Ezenyi, Salawu, Kulkarni, & Emeje, 2014), anti-inflammatory (Hanh, Hang, Van Minh, & Dat, 2011), and antibacterial (Marianne, Lesatri, Sukandar, Kurniati, & Nasution, 2014; Atindehou, Lagnika, & Guerold, 2013) properties. Despite its huge potential, bioavailability of its essential bioactive substance (*Cromaloena Odorata*) is relatively low due to poor aqueous solubility and absorption (Benjamin, 2015; Putri, & Fatmawati, S. 2019). The condition can cause no effects of *cromaloena odorata* compounds in the body. Incorporation of *cromaloena odorata* extract into PVA-based nanofiber is therefore expected to enhance the

*Correspondence Address:

Jl. Prabumulih-Palembang Km 32 Inderalaya, Ogan Ilir 30662
E-mail: ida_sriyanti@unsri.ac.id

solubility and bioavailability of cromaloena odorata.

One of the method to produce nanofiber is electrospinning (Sriyanti et al., 2017a; Sriyanti, Edikresnha, Munir, Rachmawati, & Khairurrijal, 2017b; Munir, Suryamas, Iskandar, & Okuyama, 2009; Sriyanti et al., 2018). In electrospinning process, the solution will be induced charge. The solution is usually loaded into a syringe and ejected from a needle which is connected to the high voltage source. If the electrostatic force is higher as the surface voltage with electric, the Taylor cone will be formed. When the electrostatic force from the electric charge is higher than the surface voltage, the emission from the end of the needle caused the liquid out of the nozzle towards the collector and produce the fiber that deposited on a grounded collector. The properties of nanofiber produced by electrospinning process is determined by several factors related to solution, process, and environment (Ramakrishna, Fujihara, Teo, Lim, & Ma, 2005). The solution parameters include the polymer molecular weight, viscosity, conductivity, and surface tension (Ramakrishna et al., 2005). A large number of studies has explored the solution parameter including variation of polymer concentration for production of vinyl polymer-based nanofiber, such as PVP/indomethacin (Rasekh et al., 2014), PVA/meloxicam (Samprasit et al., 2015) and PVP/GME (Sriyanti et al., 2017a; Sriyanti et al., 2018) for drug delivery system, also Chitosan-ethylenediaminetetraacetic acid/polyvinyl alcohol (CS-EDTA/PVA) for cosmetics (Charernsriwilaiwat, Rojanarata, Ngawhirunpat, Sukma, & Opanasopit, 2013). However, there is no available information regarding electrospinning process for PVA/COE nanofiber with various process parameters including electric voltage, solution flow rate and TCD in the literature yet. The parameters are very important because it is associated with the fibers diameter and the molecular interaction between the polymer and the active substance.

In this study, we have evaluated the there important process parameters, spinning voltage, flow rate and TCD, on the morphology of the PVA/COE fiber. In addition, we evaluated the intermolecular interaction in PVA/COE that has potential application as antimicrobial wound dressing.

METHODS

Methods. The research method has

been used in this research is inductive method, that is started with literature study, observation (experiment and characterization) and analysis, while the synthesis method used is electrospinning method. The Electrospinning is the most versatile method for nanofibers syntheses. The Electrospinning offers great capability in producing fibers ranging from very small diameter to 100 nm or greater and presents good mechanical characteristics and controlled surfaces.

Materials. Poly(vinylalcohol), Cromaloena Odorata leaf (obtained from local market in Palembang, Indonesia), aqua demineralization from Palembang, and the ethanol from Bratachem, Indonesia.

Precursor solution preparation. PVA/COE nanofiber was made from initial solution that has been prepared using in-situ method. 10% (w/w) of COE was dissolved in aqual and stirred at 37 °C for five hours. Separately, 10% (w/w) of PVA was dissolved in ethanol and stirred at 40°C for two hours. These two solutions were mixed to reach a mass ratio of PVA to COE of 10:5 and was stirred at 37 °C for 60 minutes.

Electrospinning process. The homogenous solution was put into 10 ml syringe with needle diameter of 0.8 mm. The parameters for nanofiber synthesis process was optimized by varying the flow rate, voltage and TCD of solution. The setup of electrospinning process is shown in Figure 1. Three different flow rate were used: 0.1, 0.5 and 1 μ L/minute with constant voltage of 10 kV and TCD of 12 cm. For the optimization of voltage in PVA/COE electrospinning process, we varied the voltage at 10, 14 and 18 kV with constant flow rate of 0.5 μ L/minute and TCD of 12 cm. The TCD (8, 12 and 16 cm) with constants flow rate of 0.5 μ L/minute and voltage of 10 kV.

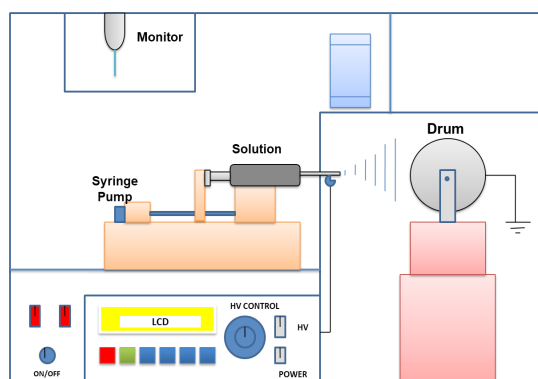


Figure 1. Electrospinning setup

The setup of electrospinning process is

shown in Figure 1, consisting of a syringe pump to discharge polymer solution from the syringe needle, high voltage power supply to induce fiber formation, and a drum collector to collect fibers. In electrospinning technique, a high voltage is generated between the polymer solution contained in a syringe needle and drum collector. The polymer solution transformed from liquid phase to solid phase or fibers.

Morphology and Size. Scanning Electron Microscopy (SEM) technique was used to analyze the morphology of PVA/COE nanofibers. The fiber was coated with gold to improve conductivity. Image scanning was performed on scanning electron microscope (JEOL, JSM-6560) at 15 kV and 10000-fold optical magnification. SEM images were analyzed further for determination of fiber diameter. Average fiber size was obtained by measuring diameter of fiber taken from one hundred points using Image J software.

Physicochemical characteristics. Fourier Transform Infrared Spectroscopy (FTIR) was used to identify possible intermolecular interaction between PVA and COE. The KBr discs method was used for all PVA/COE fibers. Samples were analyzed with FTIR spectrophotometer (Bruker, Alpha) and the spectrum scanning was performed from 500 to 4000 cm^{-1} .

RESULTS AND DISCUSSION

Electrospinning Process.

The PVACOE solution of PVA/COE was formed into nanofiber via electrospinning process for 8-10 hours with various voltages and flowrates. In the electrospinning process, the charge will be induced into the solution when the needle is connected to a high voltage source. If the amount of charge is proportional to the surface tension it will form a Taylor cone. When the load exceeds the surface tension, there is an emission from the TID of the needle that causes the liquid to pull out of the tip of the needle. The charged jets undergo the process of withdrawal and will produce of fiber (Ramakrishna, 2005). The fibers collected on the rotating collector are PVA/COE nanofiber, can be seen in Figure 2. In general, physical appearance of PVA/COE nanofibers were marked by yellowish and smooth surfaced-mats. This showed that COE were perfectly blend into PVA matrix. Nanofiber was kept in an environmentally controlled storage condition (air-tight container, 30°C with 40-50% humidity). In general, physical appearance of PVA/COE nano-

fibers were marked by yellowish and smooth surfaced-mats. This showed that COE were perfectly blend into PVA matrix. Nanofiber was kept in an environmentally controlled storage condition (air-tight container, 30°C with 40-55% humidity).



Figure 2. PVA/COE nanofiber produced from electrospinning method

Effect of the electrospinning process parameters to the fibers morphology of PVA/COE

Optimization of flow rate in PVA/COE electrospinning process, the variation were 0.1, 0.5 and 1 $\mu\text{L}/\text{minute}$. Applied voltage, TCD, and the cylinder collector rotation were constantly maintained at 10 kV, 12 cm, and 50 rpm, respectively. Figure 3(a-c) shows SEM images ($\times 10,000$) of fibers resulted from various flow rate. It was found that the morphology did not change when the flow rate was modified. The resulting of morphology are bead-free fibers. This finding is consistent with previous study that reported increased flow rate produce bead-free fiber (Song et al., 2008). At higher flow rate, the morphology of nanofiber more bigger, because more solution is drawn to the collector during electrospinning process (Ramakrishna et al., 2005). One of the important process parameter on the morphology of fiber formed is the applied voltage. The voltage associated with the charge transport in the solution during spinning process. In electrospinning, higher voltage is needed to induce the ejection of a liquid jet to form the Taylor cone (Ramakrishna et al., 2005; Sriyanti et al., 2017b). Figure 3 (d-f) shows SEM images ($\times 10,000$) of PVA/COE with TCD of 12 cm and applied flow rate of 0.5 $\mu\text{L}/\text{minute}$. The applied voltage was varied from 10, 14, and 18 kV. From the SEM images, we found that increased applied voltage affected the fiber morphology and diameter. The nanofiber produced from voltage was 10 kV condition had a long cylindrical shape with no visible flaws such as beads or fragmented strands. When applied voltage increased to 14 kV and 18 kV, there were slight changes in the morphology

of resulted fiber. As the applied voltage increased further, the jet instability in Taylor cone was more obvious (Ramakrishna et al., 2005; Song, Kim, & Kim, 2008). This instability was thought to be caused by side-jet addition formed from the solution suspended at the tip of the nozzle upon voltage induction. As a result, average fiber diameter decreased (Ramakrishna et al., 2005; Sriyanti et al., 2017a). Previous study has reported that an increase in applied voltage in polyvinyl acetate (PVAc)/ethanol (Song et al., 2008), caused a decrease in the fiber diameter.

The TCD is directly related to the magnitude of the electric field, the deposition of fibers deposition on the collector, and the evaporation of the solution. At short distance, the surrounding electric field will be larger hence reducing the time required for the fibers to be deposited on the collector and increase the rate of evaporation (Ramakrishna et al., 2005). Figure 3 (g-i) shows the SEM images (x10,000) of PVA/COE with TCD variation. The variation in TCD did not affect the morphology of the fibers and the nanofibers formed were still relatively uniform. Meanwhile, at a distance of 12 cm, the fibers were more regularly uniform which then proved that this was the optimum distance to form fibers. Similar conditions have been reported by other researchers which stated that the distance between the needle and the collector will affect the formation of regular fibers (Sultana, Hassan, & Lim, 2015)

Effect of the electrospinning process parameters to the fibers diameter of PVA/COE

Although the morphology was not affected by low rate variation, fiber diameter was found to be dependent on flow rate, as shown in Figure 4(a-c). The diameter ranged from 150 to 1200 nm with average diameter of 428 nm, 537, and 619 nm. The relationship between flow rate and fiber diameter was shown in Figure 4a. Average fiber diameter were larger as the flow rate increased. At higher flow rate, there are more solution suspended at the tip of the nozzle while elongation time is constant (Ramakrishna et al., 2005). This finding is consistent with previous study that reported increased PVAc fiber size due to increasing flow rate (Song et al., 2008).

As mentioned earlier, applied voltage not only affected fiber morphology but also fiber diameter. The average diameter of nanofiber at applied voltage of 10, 14, and 18 kV were 537, 504, and 458 nm, respectively. Increased ap-

plied voltage resulted in smaller fiber diameter, as shown in Figure 4(d-f). Smaller diameter is a direct result of smaller Taylor cone, which is induced by higher voltage. At higher voltage, electrostatic force is stronger and thus Taylor cone formation occurred on a higher rate, resulting in smaller cone jet volume (Ramakrishna et al., 2005). Therefore, we can conclude that variation of applied voltage affected fiber diameter by altering cone volume.

Another effect that occurred due to the changing distance between TCD was the diameter of the fiber. The distribution of fibers diameter can be seen in Figure 4(g-i). At the distance of 8, 12, and 14 cm, the average diameters were 619 nm and 537 nm, 449 nm, respectively. The relationship between the gap size to diameter of fibers is presented in Figure 4c. When the gap was large, the diameter of fibers was smaller. This happened since the increasing size of the gap will stretch the solution jet more since the travel time of the fibers will be longer as well (Ramakrishna et al., 2005).

The effect of the process parameters to the molecular interaction of PVA/COE

The infrared spectrum formed by PVA with molecular formula $(C_6H_9NO)_n$ can be seen in Figure 5a. The wide peak at wave number 3400 cm^{-1} shows the O-H stretching of hydroxyl group. The presence of PVA molecules was characterized by a sharp peak at wave number of 1659 cm^{-1} which shows the C = C stretching of cyclic amide groups and also the peaks at wave numbers of 816 cm^{-1} which show the stretching of C-O bend. The peak at wave number of 2840 cm^{-1} and 2920 cm^{-1} indicates the asymmetrical and anti-asymmetrical stretch of CH₂ while the peak at wave number of 1365 cm^{-1} shows the deformation of S=O group (Awada & Daneault, 2015; El-aziz, El-Magraby & Taha, 2016). Meanwhile, the FTIR results of COE is also shown in Figure 5a. The peaks characteristic of COE can be observed at wave numbers 3342, 1639, 1453 and 1043 cm^{-1} which respectively represent the strain of O-H stretching of hydroxyl group, attributed to the presence of protein amide I, N-H bending, and carbohydrate (C-O-C) (Alara, & Abdurahman, 2019). In general, the spectra obtained from the COE indicated the presence of hydroxyl group showing the presence of phenolic compounds (Alara, Abdurahman, & Ukaegbu, 2018).

FTIR is a technique to determine the IR absorption for identify specific functional group

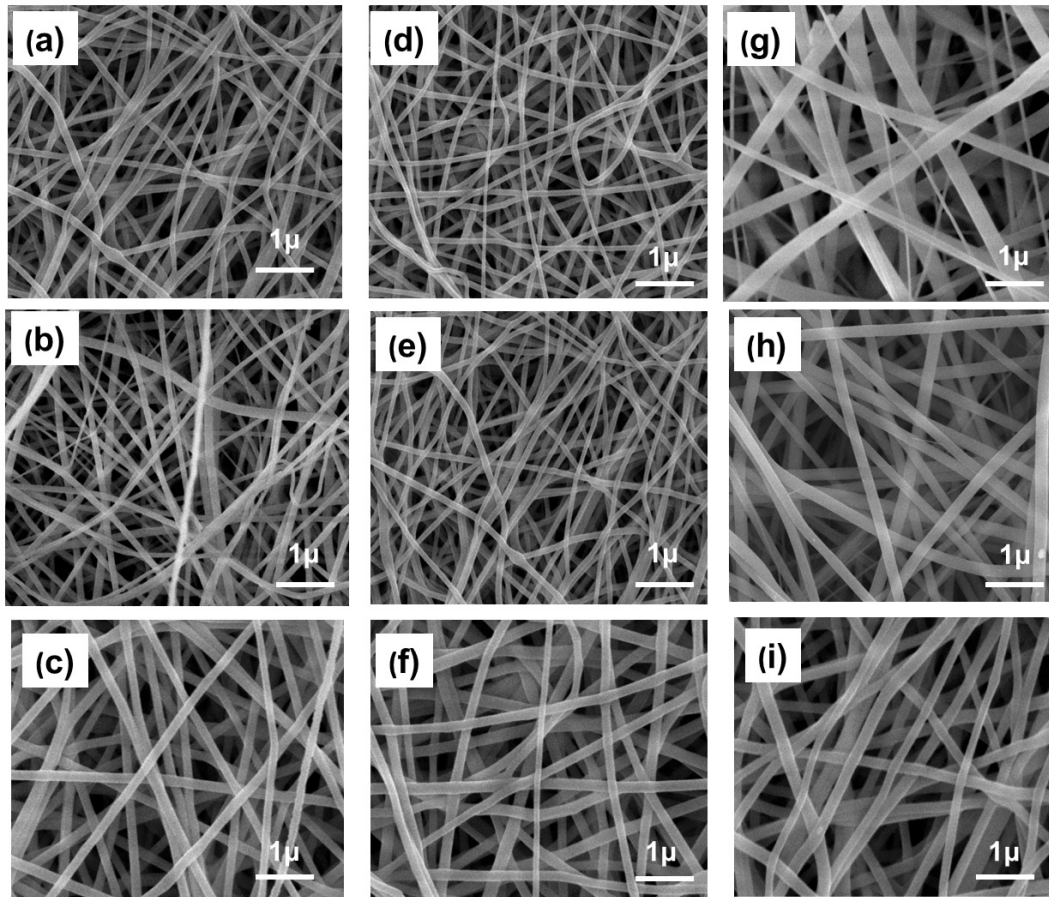


Figure 3. Scanning Electron Microscopic observation at massa rasio with variation of (a-c) flow rate (0.1 mL/h, 0.5 mL/h, 1 mL/h), (d-f) voltage (10 kV, 14 kV, 18 kV) and (g-i) TCD (8 cm, 12 cm, 16 cm)

and the molecule interaction. Figure 5b illustrated the FTIR spectrum of PVA/COE nanofiber with variatio flow rate 0.1, 0.5, 1 mL/h. An decreases in flow rate caused the peak shifting toward higher wavenumber from 3401 cm^{-1} to 3395 cm^{-1} . This peak belongs to O-H stretching from the hydroxyl group that indicate as strong hydrogen chemical bond (Awada & Daneault, 2015; El-aziz, El-Magraby & Taha, 2016). A peak appeared around 2930-2932 cm^{-1} was identified as asymmetric C-H stretching from alkanes group. This peak became broader and the shifted to higher wavenumber. This indicated higher bonding energy between C-H. Additionally, a strong peak at 1590 cm^{-1} assigned for C=C stretching (aromatic) shifted to 1594 cm^{-1} . At 813 cm^{-1} , a peak of In-plane C-O-S bond from FFG1 nanofiber was observed. Peak shift of aromatic group indicated C = C intermolecular interaction between COE and PVA. FTIR peak assignment for peak Assignment of PVA/COE nanofiber with variatio flow rate 0.1, 0.5, 1 $\mu\text{L}/\text{minute}$ are shown in Table 1.

FTIR is a very useful technique to identify specific functional groups present in PVA/COE fiber. The spectrum of variation voltage 10, 14, 18 kV fiber are shown in Figure 5c. Peak assignment of variation voltage 10, 14, 18 kV are summarized in table 1. It was found that an increase in applied voltage caused shift of a number of peaks. In general, all fiber demonstrated a broad absorption band around 3100-3800 cm^{-1} , which belongs to O-H stretching. However, this peak shifted toward lower wavenumber (3374 cm^{-1} \rightarrow 3366 cm^{-1}) when applied voltage increased, indicating weak hydrogen bonding. This can be explained by theoretical assumption where the residue of solvent used in electrospinning process (ethanol or water) was lower when higher voltage was applied (Ramakrishna et al., 2005). Consequently, less hydroxyl groups was identified by FTIR (Rahma et al, 2016; Sriyanti et al., 2017b; Sriyanti et al., 2018). Additionally, the peaks appeared around 2800-3000 cm^{-1} was assigned for asymmetric C-H stretching from

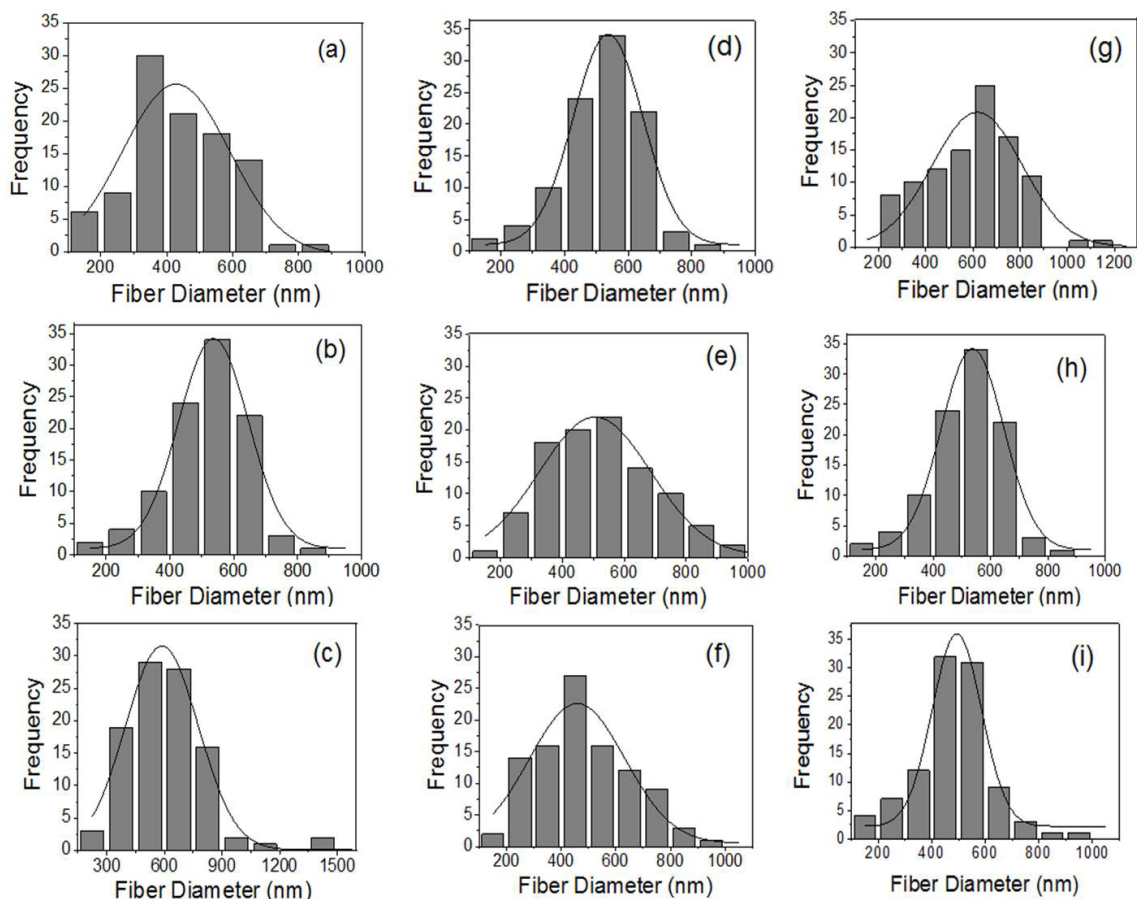


Figure 4. Fiber diameter with variation of (a-c) flow rate (0.1 mL/h, 0.5 mL/h, 1 mL/h, (d-f) voltage (10 kV, 14 kV, 18 kV) and (g-i) TCD (8 cm, 12 cm, 16 cm)

Table 1. FTIR peak Assignment of PVA/COE nanofiber with variatio flow rate 0.1, 0.5, 1 μ L/minute (Awada & Daneault, 2015; El-aziz, El-Magraby & Taha, 2016)

0.1 μ L/minute	0.5 μ L/minute	1 μ L/minute	Vibrational Mode
3401	3396	3395	O-H stretching
2841	2842	2843	Asymmetry stretch of CH ₂ pyrrole ring in alkanes
			Antiasymmetry stretch of CH ₂ pyrrole ring in alkanes
2930	2931	2932	
1590	1593	1594	C=C stretching (aromatic)
1365	1365	1366	S=O group
813	811	810	In-plane C-O-S Bond

Table 2. FTIR peak Assignment of PVA/COE nanofiber with variation voltage 10, 14, 18 kV (Awada & Daneault, 2015; El-aziz, El-Magraby & Taha, 2016)

10 kV	14 kV	18 kV	Vibrational Mode
3368	3379	3384	O-H <i>stretching</i>
2844	2945	2945	Asymmetry stretch of CH ₂ pyrrole ring in alkanes
2931	2931	2932	Antiasymmetry stretch of CH ₂ pyrrole ring in alkane
1589	1580	1578	C=C <i>stretching</i> (alkenes)
1366	1366	1365	S=O group
818	817	817	In-plane C-O-S Bond

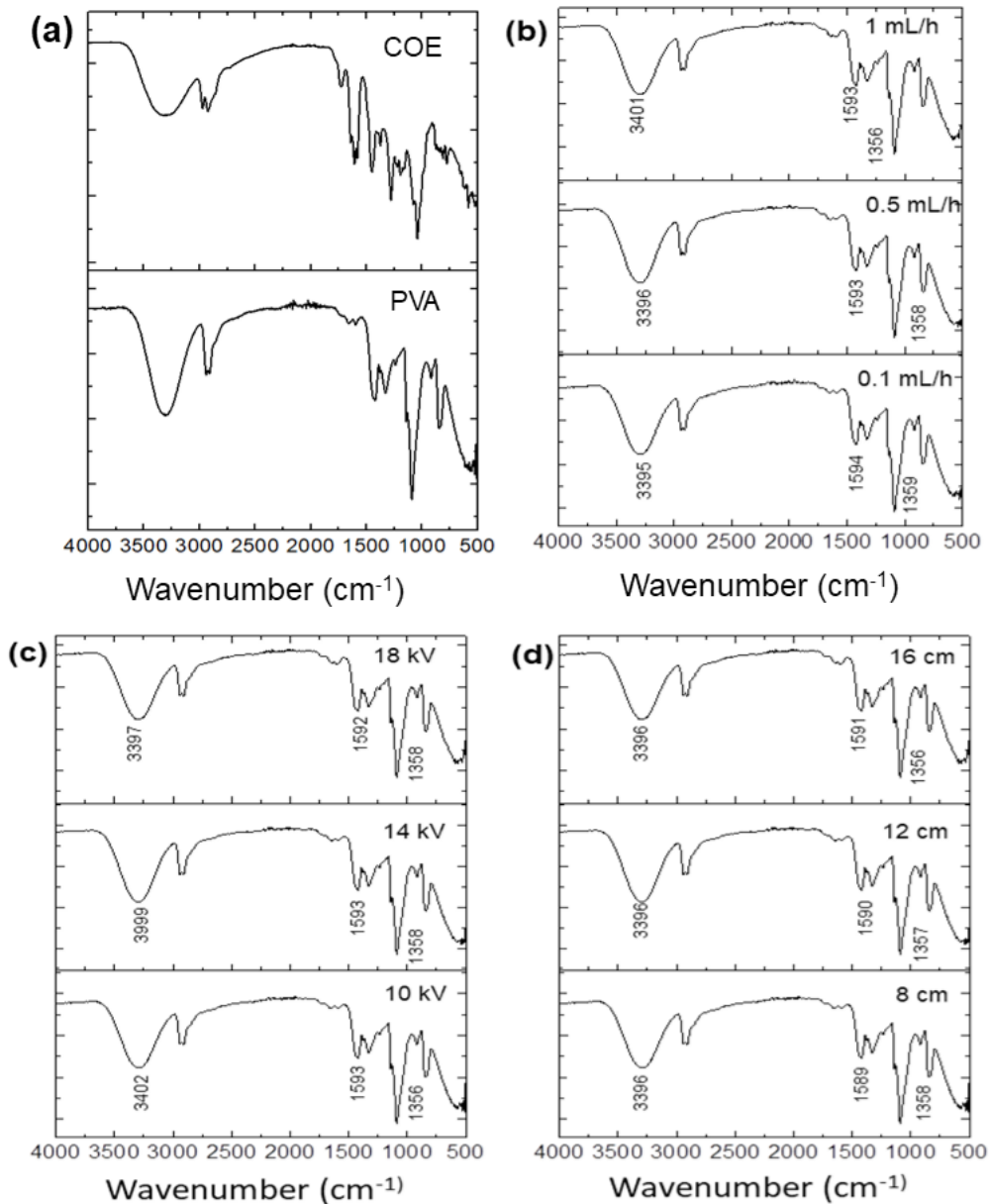


Figure 5. FTIR spectrum of (a) PVA powder and COE, (b) PVA/COE nanofiber; (c) variation flow rate 0.1, 0.5, 1 μ L/minute, (c) variation voltage 10, 14, 18 kV and (d) variation TCD of 8, 12, 16 cm

alkanes group. Higher applied voltage resulted in a broad peak with lower intensity and slightly shifted to lower wavenumber. This finding indicates lower energy bond between C-H. However, from Figure 5c it can be seen that other peaks were not affected by modification of applied voltage.

FTIR was used to detect specific groups of PVA/COE. Figure 5d shows FTIR spectra of the fibers with as the results of the varying distance of the needle to the collector at 8, 12 and 16 cm. The increasing gap size in the electrospinning process shifted the peak

of OH (hydroxyl group) bonding from 3992 cm⁻¹ to 3401 cm⁻¹ and the peak of the CH₂ pyrrole ring bonds (alkanes) from 2940 to 2943 cm⁻¹. Hence, the wave numbers shifted from lower to higher wave numbers. This is due to the interaction and the formation of intermolecular hydrogen bonds between the functional groups and the PVA group and the functional group a group of COE. Meanwhile, with the increasing distance of the needle to the collector, the peak of C = C shifted from 1589 cm⁻¹ to 1578 cm⁻¹. The peak of C=C shifted toward higher wave numbers (meaning low energy). The disappe-

Table 3. FTIR peak Assignment of PVA/COE nanofiber with varying TCD to be 8, 12, 16 cm (Awada & Daneault, 2015; El-aziz, El-Maghraby & Taha, 2016)

8 cm	12 cm	16 cm	Vibrational Mode
3392	3394	3401	O-H <i>stretching</i>
2940	2942	2943	Asymmetry stretch of CH ₂ pyrrole ring in alkanes
2951	2952	2952	Anti-asymmetry stretch of CH ₂ pyrrole ring in alkanes
1592	1591	1591	C=O <i>stretching</i> (alkenes)
1363	1362	1362	C-H deformation from CH ₂
810	811	811	In-plane N-C =O Bend

arance of the peaks of amino group showed that the intermolecular hydrogen bonding in PVA and COE weakened further. The conclusion about FTIR analysis on the peaks of PVA/COE with varying distance between the needle to collector can be seen in Table 3.

CONCLUSION

Optimization of process parameter has resulted in nanofiber with excellent morphology. The increased applied voltage affected the fiber morphology and diameter, when applied voltage increased to 14 kV and 18 kV, there were slight changes in the morphology of resulted fiber. Modification of flowrate and TCD were found to affect fiber diameter PVA/COE nanofiber. Fiber diameter decreased when higher voltage, lower flowrate and longer TCD was applied. The average diameter of nanofiber at applied voltage of 10, 14, and 18 kV were 537, 504, and 458 nm. The average diameter of nanofiber at flow rate of 0.1, 0.5 and 1 mL/jam were 428 nm, 537, and 619 nm. The average diameter of nanofiber TCD of 8, 12, and 14 cm were 619 nm and 537 nm, 449 nm. Higher applied voltage resulted in a broad peak with lower intensity and slightly shifted to lower wavenumber. The peak shift was thought to be a result of intermolecular interaction between PVA and COE via hydrogen bond formation. However, further studies are required to investigate other aspects such as mechanical strength, physical and chemical degradation. In addition, processing condition for a larger scale might require further optimization.

ACKNOWLEDGMENT

This research was financially supported by Universitas Sriwijaya, Republic of Indonesia, under the University's Grant in the fiscal year 2020.

REFERENCES

- Abd El-aziz, M. A., El-Maghraby, A., Nahla A., & Taha N. A. (2016). Comparison between polyvinyl alcohol (PVA) nanofiber and polyvinyl alcohol (PVA) nanofiber/hydroxyapatite (HA) for removal of Zn²⁺ ions from wastewater. *Applied Sciences*, 5, 840-850. <https://doi.org/10.1016/j.arabj.2016.09.025>.
- Atindehou, M., Lagnika, L., & Guerold, B. 2013. Isolation and identification of two antibacterial agents from *Chromolaena odorata* L. active against four diarrheal strains. *Advances in Microbiology*, 03, 01, 115–121. <https://doi.org/10.4236/aim.2013.31018>
- Alara, O.R., & Abdurahman, N.H. (2019). GC–MS and FTIR analyses of oils from *Hibiscus sabdariffa*, *Stigma maydis* and *Chromolaena odorata* leaf obtained from Malaysia: Potential sources of fatty acids. *Chemical Data Collections*. <https://doi.org/10.1016/j.cdc.2019.100200>.
- Alara, O.R., Abdurahman, N.H., & Ukaegbu, C.I. (2018). Soxhlet extraction of phenolic compounds from *Vernonia cinerea* leaves and its antioxidant activity, *Journal of Applied Research on Medicinal and Aromatic Plants*. 11, 12–17. <https://doi.org/10.1016/j.indcrop.2018.06.034>
- Awada, H., & Daneault, C. (2015). Chemical modification of Poly(Vinyl Alcohol) in Water. *Applied Sciences*, 5, 840-850. <https://doi:10.3390/app5040840>
- Benjamin, V. (2011). Phytochemical and Antibacterial Studies on The Essential Oil of *Eupatorium Odoratum*. *Pharmaceutical Biology*. 227. <https://doi.org/10.3109/13880208709060911>
- Charemsriwilaiwat, N., Rojanarata, T., Ngawhirunpat, T., Sukma, M., & Opanasopit, P. (2013). Electrospun chitosan-based nanofiber mats loaded with *Garcinia mangostana* extracts. *International Journal of Pharmaceutics*, 452, 333–343. <https://doi.org/10.1016/j.ijpharm.2013.05.012>
- Dai, X. Y., Nie, W., Wang, Y. C., Shen, Y., Li, Y., & Gan, S. J. (2012): Electrospun emodin Polyvinyl alcohol blended nanofibrous membrane: A novel medicated biomaterial for drug delivery and accelerated wound healing. *Journal*

- of Materials Science: Materials in Medicine*, 23 (11), 2709–2716. <https://doi.org/10.1007/s10856-012-4728-x>
- De Oliveira, J. A. M. ., Bernardi, D. I. ., Balbinot, R. B. (2017). Chemotaxonomic value of flavonoids in *Chromolaena congesta* (Asteraceae). *Biochemical Systematics and Ecology*, 70,7–13. <https://doi.org/10.1016/j.bse.2016.10.013>
- Ezenyi, I. C., Salawu, O. A. ., Kulkarni, K., & Emeje, M. (2014) . Antiplasmodial activity-aided isolation and identification of quercetin^{4'}-methyl ether in *Chromolaena odorata* leaf fraction with high activity against chloroquine-resistant *Plasmodium falciparum*. *Parasitology Research*, 113, 12, 4415–4422. <https://doi.org/10.1007/s00436-014-4119>
- Guo, M., Wang, X., Lu, X., Wang, H., & Brodelius, P. E. (2016): α -Mangostin Extraction from the native mangosteen (*Garcinia mangostana* L.) and the binding mechanisms of α -mangostin to HSA or TRF. *PLoS one*, 11, e0161566. <https://doi.org/10.1371/journal.pone.0161566>
- Handayani, G.M., Umar, I., & Ismail, S. (2018). Formulasi dan Uji Efektivitas Antioksidan Krim Ekstrak Etanol Daun Botto-Botto (*Chromolaena Odorata* L.) Dengan Metode Dpph. *Jurnal Kesehatan*, 11, 2.
- Hanh, T. T. H. ., Hang, D. T. T., Van Minh, C. ., & Dat, N. T. (2011). Antiinflammatory effects of fatty acids isolated from *Chromolaena odorata*, *Asian Pacific Journal of Tropical Medicine*, 4, 10, 760–763. [https://doi.org/10.1016/S1995-7645\(11\)60189-2](https://doi.org/10.1016/S1995-7645(11)60189-2).
- Marianne, Lesatri, D.P., Sukandar, E.Y., Kurniati, N.F., & Nasution, S. (2014). Antidiabetic Activity of Leaves Ethanol Extract *Chromolaena odorata* (L.) R.M. King on Induced Male Mice with Alloxan Monohydrate. *Jurnal Natural Unsyiah*, 14, 1, 1-4. <https://doi.org/10.24815/jn.v14i1.1382>
- Munir, M. M., Suryamas, A. B., Iskandar, F., & Okuyama, K. (2009): Scaling law on particle-to-fiber formation during electrospinning. *Polymer*, 50, 4935–4943. <https://doi.org/10.1016/j.polymer.2009.08.01>
- Naidoo, K.K., Cooposamy, R.M., & Naidoo, G. (2011). Screening of *Chromolaena odorata* (L.) king and robinson for antibacterial and antifungal properties. *Journal of Medicinal Plant Research*, 5, 19, 4859–4862.
- Opanasopit, P., Ruktanonchai, U., Suwantong, O., Panomsuk, S., Ngawhirunpat, T., Sittisombut, C., Suksamran, T., & Suphapol, P. (2008): Electrospun poly(vinyl alcohol) fiber mats as carriers for extracts from the fruit hull of mangosteen. *Journal of Cosmetic Science*, 59, 233-242.
- Pothitirat, W., Chomnawang, M. T., & Grtsanapan, W. (2010). Free radical and anti-acne activities of mangosteen fruit rind extracts prepared by different extraction methods. *Pharmaceutical Biology*, 48 (2), 182-6. <https://doi.org/10.3109/13880200903062671>
- Palakawong, C., Sophanodora, P., Pisuchpen, S., & Phongpaichit. (2010). Antioxidant and antimicrobial activities of crude extracts from mangosteen (*Garcinia mangostana* L.) parts and some essential oils. *International Food Research Journal*, 17, 583-9. <https://doi.org/10.1016/j.proche.2014.12.027>
- Park, J. Y., Lee, I. H., & Bea, G. N. (2008). Optimization of the electrospinning conditions for preparation of nanofibers from polyvinylacetate (PVAc) in ethanol solvent. *Journal of Industrial and Engineering Chemistry*, 14(6), 707–713. <https://doi.org/10.1016/j.jiec.2008.03.006>
- Putri, D.A., & Fatmawati, S. (2019). A New Flavonone as a Potent Antioxidant Isolated from *Chromolaena odorata* L. Leaves. Evidence-Based *Complementary and Alternative Medicine*. <https://doi.org/10.1155/2019/1453612>
- Ramakrishna, S., Fujihara, K., Teo, W. E., Lim, T. C., & Ma, Z. (2005): *An introduction to electrospinning and nanofibers*. World Scientific, Singapore, 3-118. https://doi.org/10.1142/9789812567611_0003
- Rahma, A., Munir, M. M., Khairurrijal, Prasetyo, A., Suendo, V., & Rachmawati, H. (2016). Intermolecular interactions and the release pattern of electrospun curcumin-polyvinylpyrrolidone) fiber. *Biological and Pharmaceutical Bulletin*, 39(2), 163–173. <https://doi.org/10.1248/bpb.b15-00391>
- Rasekh, M., Karavasili, C., Soong, Y. L., Bouropoulos, N., Morris, M., Armitage, D., & Ahmad, Z. (2014). Electrospun PVA-indomethacin constituents for transdermal dressings and drug delivery devices. *International Journal of Pharmaceutics*, 473(1–2), 95–104. <https://doi.org/10.1016/j.ijpharm.2014.06.059>
- Samprasit, W., Akkaramongkolporn, P., Ngawhirunpat, T., Rojanarata, T., Kaomongkolgit, R., & Opanasopit, P. (2015). Fast releasing oral electrospun PVA/CD nanofiber mats of taste-masked meloxicam. *International Journal of Pharmaceutics*, 487(1–2), 213–222. <https://doi.org/10.1016/j.ijpharm.2015.04.044>
- Song, J. H., Kim, H. E., & Kim, H. W. (2008). Production of electrospun gelatin nanofiber by water-based co-solvent approach. *Journal of Materials Science: Materials in Medicine*, 19(1), 95–102. <https://doi.org/10.1007/s10856-007-3169-4>
- Sriyanti, I., Edikresnha, D., Rahma, A., Munir, M. M., Rachmawati, H., & Khairurrijal, K. (2017a). Correlation between Structures and Antioxidant Activities of Polyvinyl alcohol/*Garcinia mangostana* L. Extract Composite Nanofiber Mats Prepared Using Electrospinning. *Journal of Nanomaterials*. <https://doi.org/10.1155/2017/9687896>
- Sriyanti, I., Edikresnha, D., Munir, M. M., Rach-

- mawati, H., & Khairurrijal, K. (2017b): Electrospun Polyvinyl alcohol (PVA) nanofiber mats loaded by *Garcinia mangostana* L. extracts. *Materials Science Forum*, 880, 11–14. <https://doi.org/10.4028/www.scientific.net/MSF.880.11>
- Sriyanti, I., Edikresna. D., Rahma, A., Munir, M. M., Rachmawati, H., & Khairurrijal, K. (2018). Mangosteen pericarp extract embedded in electrospun PVP nanofiber mats: physico-chemical properties and release mechanism of α -mangostin. *International Journal of Nanomedicine*. <http://dx.doi.org/10.2147/IJN.S167670>
- Sultana, N., Hassan, M. I., & Lim, M. M. (2005). *Composite synthetic scaffolds for tissue engineering and regenerative medicine*. Universiti Teknologi Malaysia. Johor bahru. <https://doi.org/10.1007/978-3-319-09755-8>.